5. Runnels, L. W., Yue, L. & Clapham, D. E. TRP-PLIK, a bifunctional protein with kinase and ion channel activities. *Science* **291,** 1043–1047 (2001).

Supplementary Information is available at *Nature*'s World-Wide Web site (http://www.nature.com) or as paper copy from the London editorial office of *Nature*.

Acknowledgements

We thank D. Tani and M. Monteilh-Zoller for technical assistance. This work was funded in part by a Beth Israel Pathology Foundation grant and a BIDMC Fireman Fellowship award to A.M.S., and a NIH grant. A.-L.P. is supported by the German Academic Exchange Service (DAAD).

Correspondence and requests for materials should be addressed to A.M.S. (e-mail: andrewms@u.washington.edu). The GenBank accession numbers for murine and human LTRPC7 cDNA and protein sequences are AY032951 and AY032950, respectively.

ADP-ribose gating of the calcium-permeable LTRPC2 channel revealed by Nudix motif homology

Anne-Laure Perraud*†, Andrea Fleig†‡, Christopher A. Dunn†§, Leigh Ann Bagley‡, Pierre Launay*, Carsten Schmitz*, Alexander J. Stokes*, Qiqin Zhu*, Maurice J. Bessman§, Reinhold Penner‡, Jean-Pierre Kinet* & Andrew M. Scharenberg*‖

** Department of Pathology, Beth Israel Deaconess Medical Center and Harvard Medical School, Boston, Massachusetts 02215, USA*
‡ Laboratory of Cell and Molecular Signaling, Center for Biomedical Research at The Queen's Medical Center and John A. Burns School of Medicine at the University of Hawaii, Honolulu, Hawaii 96813, USA
§ Department of Biology, Johns Hopkins University, Baltimore, Maryland 21218, USA
† These authors contributed equally to this work.

Free ADP-ribose (ADPR), a product of NAD hydrolysis and a breakdown product of the calcium-release second messenger cyclic ADPR (cADPR), has no defined role as an intracellular signalling molecule in vertebrate systems. Here we show that a 350-amino-acid protein (designated NUDT9) and a homologous domain (NUDT9 homology domain) near the carboxy terminus of the LTRPC2/TrpC7 putative cation channel[1] both function as specific ADPR pyrophosphatases. Whole-cell and single-channel analysis of HEK-293 cells expressing LTRPC2 show that LTRPC2 functions as a calcium-permeable cation channel that is specifically gated by free ADPR. The expression of native LTRPC2 transcripts is detectable in many tissues including the U937 monocyte cell line, in which ADPR induces large cation currents (designated I_{ADPR}) that closely match those mediated by recombinant LTRPC2. These results indicate that intracellular ADPR regulates calcium entry into cells that express LTRPC2.

The LTRPC family of putative ion channel proteins[2] has a unique amino-terminal region of 600–700 amino acids that can be divided into 4 smaller sub-regions based on their high level of conservation in one or more family members. Next there is a region of around 300 amino acids that contains the putative pore-forming transmembrane spans, and then a region with predicted coiled-coil character, and finally a C-terminal extension of variable length and unique structure for individual LTRPC members. Figure 1a illustrates the structural elements of LTRPC2, which was originally designated TrpC7 (ref. 1), but was named LTRPC2 in a recently proposed nomenclature[2].

‖ Present address: Department of Pediatrics and Immunology, University of Washington and Children's Hospital and Medical Center, Seattle, Washington 98195-6320, USA.

Whereas northern blotting indicates that LTRPC2 was dominantly expressed in brain (data not shown, consistent with previous reports[1]), polymerase chain reaction after reverse transcription of RNA (RT–PCR) detected LTRPC2 transcripts in many other tissues, including bone marrow, spleen, heart, leukocytes, liver and lung (data not shown). Specificity of the RT–PCR analysis was confirmed by cloning a full-length LTRPC2 transcript from a human monocyte complementary DNA library. On the basis of its unique C-terminal structure, we subsequently cloned a new cDNA from a spleen cDNA library, designated NUDT9. Its expression was detectable by RT–PCR in every tissue analysed, including bone marrow, spleen, heart, leukocytes, liver, lung, kidney, prostate, testis and skeletal muscle (data not shown). The C-terminal region of LTRPC2 and NUDT9 share 50% homology and are also homologous to the *Caenorhabditis elegans* predicted protein EEED8.8 (Fig. 1b). Sequence analysis of NUDT9 revealed the presence of a putative signal peptide/anchor and a Nudix box sequence motif. Nudix boxes are found in a family of diverse enzymes that catalyse the hydrolysis of nucleoside diphosphate derivatives[3]. This motif is highly conserved in EEED8.8, and is present in a less conserved form in the NUDT9 homology region (NUDT9-H) of LTRPC2.

On the basis of the presence of the Nudix box in NUDT9 and the homology between NUDT9 and LTRPC2, we thought that identifying a potential substrate for NUDT9 would provide insight into LTRPC2 function. We therefore expressed NUDT9 in *Escherichia coli*, purified the protein, and screened a series of nucleoside diphosphate derivatives for enzymatic activity. The recombinant protein was a highly specific ADPR pyrophosphatase (yielding AMP and ribose 5-phosphate) with a K_m of 100 ± 10 μM and a V_{max} of 11.8 ± 0.3 μmol min^{-1} mg^{-1} protein. We then expressed the LTRPC2. NUDT9-H in *E. coli* and evaluated its activity towards the same panel of substrates. NUDT9-H had the same specific ADPR pyrophosphatase activity and an identical K_m (100± 10 μM), but a far lower level of activity (V_{max} = 0.1 μmol min^{-1} mg^{-1}). This may be because of the substitution of RIL and QE amino acids in LTRPC2 for the conserved REF triad and EE diad found in the Nudix motifs of NUDT9 and EEED8.8, as these are important for the catalytic activity of other Nudix hydrolases[3]. However, we cannot exclude that the reduced activity of the LTRPC2 NUDT9-H domain relative to that of NUDT9 may be because it is not in its native protein context.

The simplest model to relate NUDT9/NUDT9-H activity to LTRPC2 function is to have LTRPC2 as an ion channel somehow regulated by ADPR. To test this, we used a human embryonic kidney cell line (HEK-293) with tetracycline-regulated transcription of a Flag-tagged LTRPC2 construct. As can be seen in Fig. 2a, in wild-type cells, no transcript was detectable using an LTRPC2-specific probe. After tetracycline induction of cells stably transfected with a textracycline-controlled LTRPC2 construct, substantial expression of an around 6-kilobase (kb) recombinant LTRPC2 transcript was detectable. Similarly, anti-Flag immunoreactive protein of the correct predicted molecular mass was detected in western blots only after tetracycline induction of the stably transfected cells (Fig. 2b). Finally, anti-Flag immunofluorescence indicated that a significant portion of LTRPC2 was localized at or near the plasma membrane (Fig. 2c); this led us to perform patch-clamp analyses of plasma-membrane currents. Without tetracycline induction, ADPR has no detectable effect on plasma-membrane currents (Fig. 2d). Furthermore, in the absence of ADPR in the patch pipette, basal currents in tetracycline-treated cells are the same as in wild-type HEK-293 cells. This indicates that LTRPC2 is not open constitutively under our conditions of standard intracellular solutions. In contrast, after tetracycline induction, large inward and outward currents reversing at 0 mV were induced by 100 μM ADPR (Fig. 2d; Fig. 2e, linear I–V curves at various times of current development). No current activation was observed using 100 μM of a variety of closely related molecules, including NAD^+, cADPR, ATP, ADP,

ADP-glucose, ADP-mannose, GDP-glucose, GDP-mannose, UDP-glucose and UDP-mannose, or ADPR's immediate breakdown products AMP and ribose 5-phosphate. Furthermore, no detectable gating occurred with agents that induce depletion of intracellular Ca^{2+} stores, such as 20 μM inositol 1,4,5-triphosphate or 10 μM ionomycin (data not shown). The relationship between intracellular ADPR concentration and whole-cell current magnitude (summarized in Fig. 2f) indicates that LTRPC2 gating begins at around 60–100 μM ADPR and saturates at around 300 μM with an effector concentration for half-maximum response (EC_{50}) of 90 μm. The EC_{50} for channel gating is similar in magnitude to the enzymatic K_m of both NUDT9 and LTRPCP2 NUDT9-H, consistent with the hypothesis that this domain is directly involved in the ADPR-induced effects.

The LTRPC2 structure and linear *I–V* curve reversing at 0 mV both indicate that LTRPC2 functions as a non-specific cation channel. To analyse its permeation selectivity more directly, we measured ADPR-induced currents in whole cells and briefly applied solutions with isotonic substitutions for specific extracellular cations. The inward component of ADPR-induced whole-cell currents was suppressed when cells were perfused extracellularly with isotonic *N*-methyl-D-glucamine chloride (Fig. 3a) or choline-chloride (not shown). Similar experiments, using isotonic Ca^{2+} solutions (120 mM $CaCl_2$) revealed the ability of Ca^{2+} ions to maintain approximately 50% of the inward current observed using the standard extracellular solution (Fig. 3b). These data indicate that LTRPC2 functions as a non-selective cation channel that is permeant to both Na^+ and Ca^{2+}.

To address the question of whether ADPR directly affects LTRPC2 function, we tested the ability of ADPR to induce LTRPC2-gating in cell-free, inside-out patches. As shown in Fig. 3c, under the same conditions used for the whole-cell analyses, channel openings were easily detectable, within seconds of brief applications of ADPR to the inside surface of patches excised from induced HEK-293 cells, but not from patches excised from uninduced cells. Channels opened with concentrations of ADPR as low as 10 μM, albeit in only one out of five patches. At concentrations of 30 μM or higher, ADPR consistently gated multiple channels in all patches ($n = 12$). Remarkably, brief applications of ADPR resulted in sustained channel openings for periods of up to 1–2 min even after ADPR exposure was stopped; this may in part contribute to the high apparent cooperativity of LTRPC2's dose–response curve for ADPR. Channel activity could be induced repetitively and reversibly in the same patch for up to 20 min with no obvious signs of decreased activity. We also analysed the channel activity using symmetric NaCl-based solutions on each side of the patch mem-

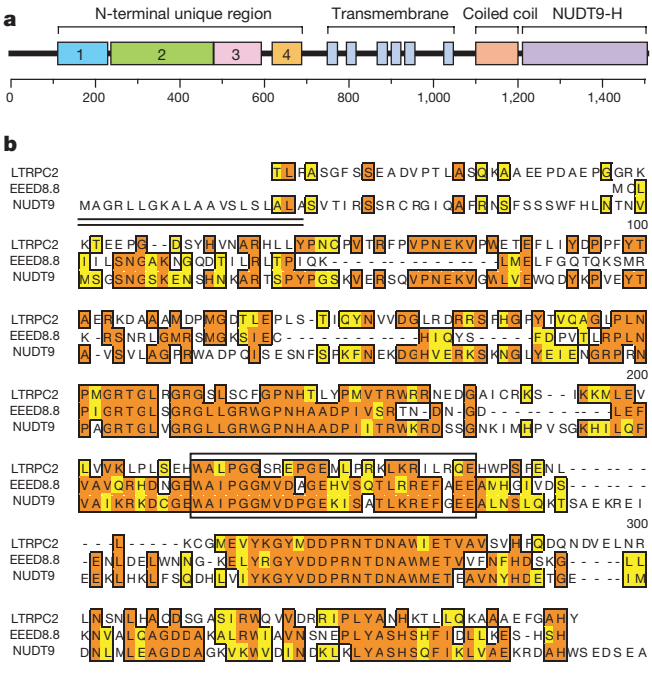

Figure 1 Protein sequence analysis of LTRPC2. **a**, Schematic of LTRPC2 structural motifs on the basis of alignments of various related proteins including MLSN-1, LTRPC7, MTR-1 and the *C. elegans* proteins C05C12.3, T01H8.5 and F54D1.5. **b**, ClustalW alignment of the NUDT9 homology region of LTRPC2, EEED8.8 and NUDT9. The putative signal peptide or anchor found in NUDT9 is double underlined (prediction on the basis of SignalP2.0 analysis of the NUDT9 amino-acid sequence). The Nudix box region is boxed by a rectangle.

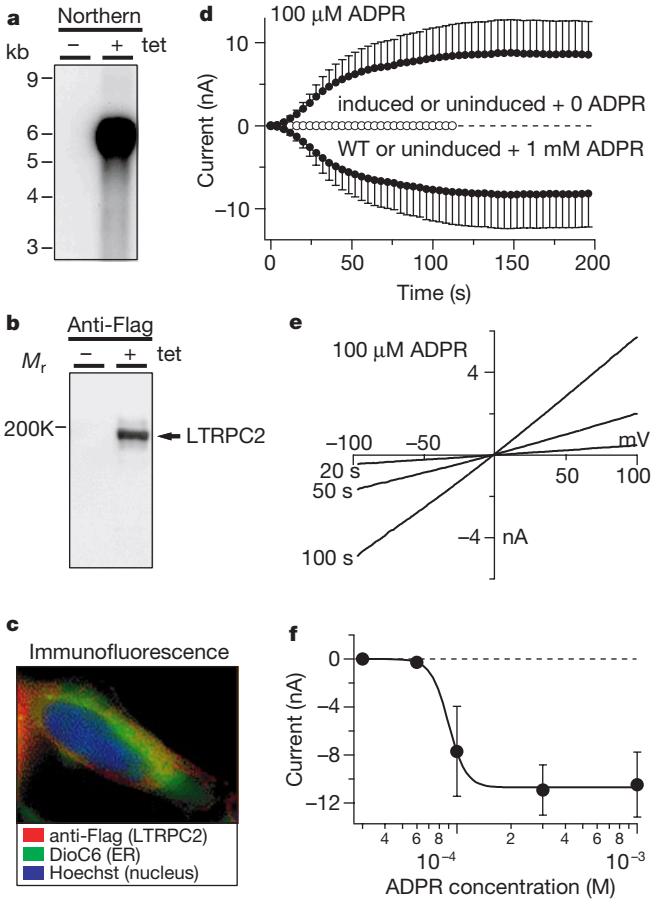

Figure 2 Functional expression of LTRPC2 in HEK-293 cells. **a**, Non-transfected wild-type or tetracycline-induced HEK-293 cells (1 μg ml^{-1}, 24 h) were analysed by northern blot using a human LTRPC2 probe. Recombinant LTRPC2 is revealed as an ~5.5-kb messenger RNA. **b**, HEK-293 cells were treated or not for 24 h with 1 μg ml^{-1} tetracycline. Cells (10^6) were analysed for expression of a Flag-reactive protein by anti-Flag immunoprecipitation/anti-Flag immunoblotting. **c**, Representative HEK-293 cell after tetracycline induction of Flag-LTRPC2 expression and staining with anti-Flag monoclonal antibody (red), DioC6 (green, perinuclear endoplasmic reticulum) and Hoechst (blue, nucleus). Peripheral red staining indicates LTRPC2 in the plasma membrane. **d**, Temporal development of averaged membrane currents at –80 and +80 mV. Only tetracycline-induced HEK-293 cells expressing Flag–LTRPC2 generated large inward and outward currents when perfused with 100 μM ADPR ($n = 4 \pm$ s.e.m., filled symbols). Open symbols represent superimposed analyses of responses from wild-type or uninduced HEK-293 cells perfused with or without 1 mM ADPR ($n = 3$–5). **e**, *I–V* relationships of ADPR-induced currents at different times after break in a representative cell perfused with 100 μM ADPR. **f**, Dose–response curve for ADPR-dependent gating of LTRPC2 on the basis of average currents at –80 mV ($n = 5$–$12 \pm$ s.e.m.), yielding an apparent EC_{50} of 90 μM and a Hill coefficient of 9 (Hill coefficients of 4–8 yielded similarly adequate approximations).

brane (Fig. 3d), with $[Ca^{2+}]_i$ buffered to 100 nM and with the solution facing the inside patch surface supplemented with 100 μM ADPR. Again, single-channel events were readily detected upon patch excision into this solution ($n = 8$); however, under these conditions, the probability of channel opening was voltage dependent, with shorter channel opening times observed at negative potentials. The single-channel current–voltage relationship is shown in Fig. 3e and linear regression through the open levels of single-channel events yielded a slope conductance of 60 pS. Because the voltage dependence exhibited by single channels under these symmetrical Na^+-based conditions had not been observed in our previous whole-cell analyses, we measured whole-cell currents using these ionic conditions. We observed a corresponding voltage-dependent deactivation of whole-cell currents on a seconds time scale at negative potentials (Fig. 3f). This shows that the behaviour of macroscopic ADPR-induced currents mirrors that observed for ADPR-gated single channels. These results provide compelling evidence that ADPR directly gates LTRPC2.

The data indicate that free ADPR may be able to regulate calcium entry by directly gating LTRPC2, and they also provide several elements that may be used to identify native calcium-entry pathways that use this mechanism. However, there are neither published reports linking ADPR to calcium entry nor any reports of native ADPR-induced membrane currents in mammalian systems. As the source of our LTRPC2 cDNA clone was a cDNA library of human monocytes, we evaluated the human U937 monocyte cell line for expression of LTRPC2 transcripts by northern blotting. As illustrated in Fig. 4a, we detected a transcript in U937 cells that was slightly larger than that of our inducible LTRPC2-expressing HEK-293 cell line, and this was consistent with the predicted 6.2 kb size of the native LTRPC2.

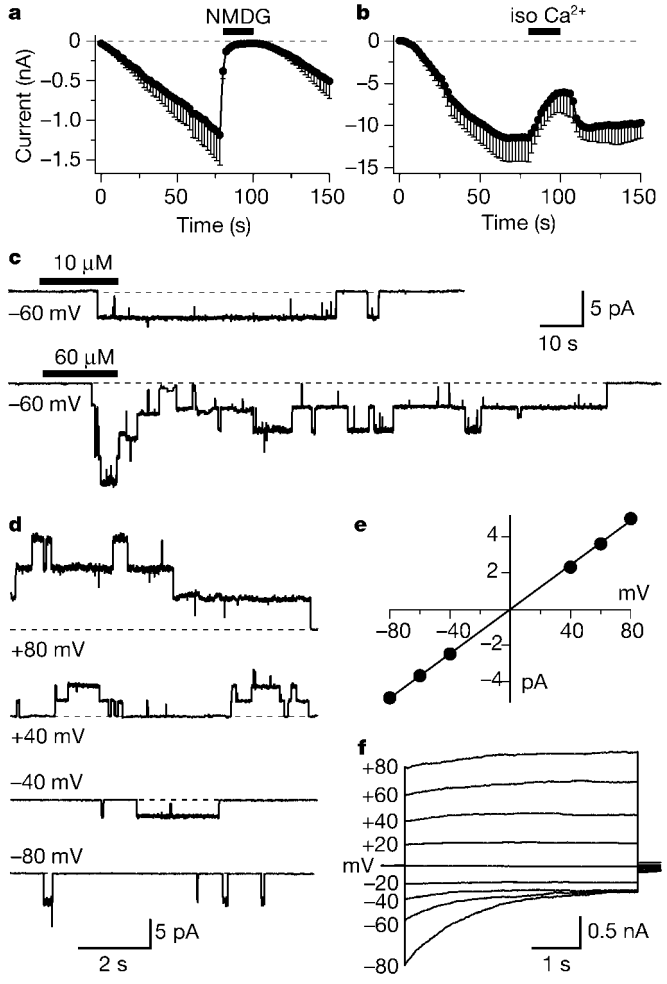

Figure 3 Permeation and single-channel properties of LTRPC2. **a**, HEK-293 cells expressing Flag–LTRPC2 were perfused with 300 μM ADPR. Experiments were performed on cells after 16 h induction, resulting in smaller average current amplitudes. At the time indicated by the bar, isotonic NMDG-Cl solution (180 mM NMDG-Cl, 330 mOsm) was applied externally ($n = 3$). **b**, Same as **a**, except that isotonic $CaCl_2$ solution (120 mM $CaCl_2$, 300 mOsm) was applied ($n = 3$), supporting about 50% of current previously carried by Na^+. **c**, Reversible activation/deactivation of LTRPC2 by 10 μM and 60 μM ADPR, briefly applied to inside-out patches using Cs-glutamate-based internal and NaCl-based external solutions. Channel open times were extremely long under these recording conditions. **d**, LTRPC2 channels recorded under symmetrical Na^+-based solutions with 100 μM ADPR added to the internal solution. There was an apparent voltage dependence of channel opening probability. **e**, Single-channel *I–V* relationship derived from averages of several events from different patches ($n = 3$–12), yielding a single-channel conductance of 60 pS. **f**, Average whole-cell currents using the same solutions as in **d**. At negative potentials the channels inactivated to a steady-state plateau, whereas positive potentials recruited more channels over time ($n = 6$).

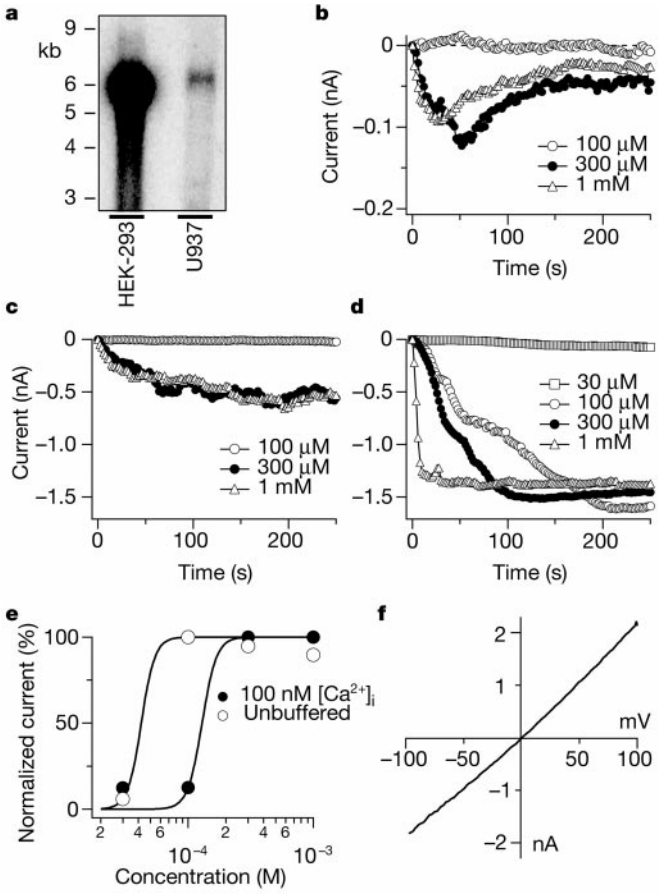

Figure 4 ADPR-gated cation currents in human U937 cells. **a**, Northern blot analysis identifies LTRPC2 as a 6 kb mRNA in tetracycline-induced HEK-293 cells (1 μg ml^{-1}, 24 h) and in native U937 cells. This blot was exposed for a longer time to provide optimal detection of the native transcript, causing overexposure of the recombinant transcript. **b**, Inward currents in U937 cells at –80 mV activated by different intracellular concentrations of ADPR in the presence of 10 mM BAPTA ($n = 4$–11 each). **c**, Same as **b**, except that $[Ca^{2+}]_i$ was buffered to 100 nM ($n = 5$–7 each). **d**, Same as **b** and **c** in the absence of exogenous buffers ($n = 5$–9 each). **e**, Dose–response relationships for I_{ADPR} in U937 cells perfused with defined ADPR concentrations while $[Ca^{2+}]_i$ was buffered to 100 nM (filled symbols) or left to vary freely by omitting exogenous buffers (open symbols), yielding an apparent EC_{50} of 130 μM and 40 μM for buffered and unbuffered conditions, respectively (in both cases, Hill coefficients were 8). **f**, I–V relationship of ADPR currents in U937 cells. Representative current records in response to a voltage ramp ranging from –100 to +100 mV over 50 ms, obtained with 100 μM ADPR under unbuffered conditions.

We performed whole-cell patch-clamp analyses of U937 cells with varying amounts of ADPR present in the intracellular solution (Fig. 4b). Once the whole-cell configuration was established, inward currents developed rapidly if ADPR was present in the patch pipette. Under these experimental conditions, in which 10 mM BAPTA was employed to buffer $[Ca^{2+}]_i$ to zero, the EC_{50} of ADPR was around 130 μM, comparable with the amount required for gating of LTRPC2 in the recombinant system (90 μM). The currents produced by ADPR (designated I_{ADPR}) were small with an inactivation that was time-dependent. This inactivation was not observed, and current amplitudes were significantly larger, when free $[Ca^{2+}]_i$ was buffered to 100 nM with BAPTA (Fig. 4c). This indicates that I_{ADPR} may possess some degree of Ca^{2+}-dependence with a decreased probability of channel opening when BAPTA-containing pipette solutions are equilibrated with the cytosol and clamp $[Ca^{2+}]_i$ to zero. This interpretation is further supported by experiments in which $[Ca^{2+}]_i$ was left to vary freely (that is, omitting BAPTA and leaving cytosolic Ca^{2+} concentrations unbuffered). These conditions led to an I_{ADPR} developing more rapidly and of an even larger magnitude (Fig. 4d). Dose–response curves for ADPR revealed a similar steepness to that observed for recombinant LTRPC2 channels and, under unbuffered conditions, there was a significant leftward shift of the dose–response curve to ADPR (yielding an EC_{50} of 40 μM; Fig. 4e). We observed a similar sensitization in the LTRPC2-expressing HEK-293 cells by $[Ca^{2+}]$ (data not shown) and noticed a larger degree of variability in responses in both HEK-293 and U937cell systems, as would be expected when $[Ca^{2+}]_i$ was left to vary freely. Regardless of the above experimental conditions, I_{ADPR} had a linear I–V relationship reversing at 0 mV that was indistinguishable from that observed with currents carried by heterologously expressed LTRPC2 (Figs 4f and 2f).

In summary, our results provide converging biochemical and electrophysiological evidence that ADPR can regulate calcium entry in vertebrate systems through its ability to gate LTRPC2 directly. They also provide significant insight into LTRPC2 structure/function by raising the possibility that the NUDT9-H domain of LTRPC2 can function as an ADPR binding site and/or act as an intrinsic deactivation mechanism for LTRPC2 through its ability to break down ADPR. Our results provide an unequivocal molecular link between ADP-ribose and calcium entry into a mammalian system. It has been reported that ADPR gates the fertilization channel of ascidian oocytes[4], but differences in single-channel conductance as well as the differential effects of intracellular Ca^{2+} buffering seem to set these two ion channels apart. As free ADPR is produced in many contexts, for example, through the pyridine nucleotide cycle, apoptosis, cytosolic and ecto-NAD glycohydrolases, cADPR breakdown and within mitochondria[5–12], ADPR-mediated gating of LTRPC2 may have numerous roles in cellular function. □

Methods

RT–PCR and northern blot analysis of expression

For PCR analysis of LTRPC2 expression, we used the primers CAGTGTGGCTACACGCATGA and TCAGGCCCGTGAAGACGATG to obtain a 138-base pair (bp) band. For NUDT9 expression, we used the primers GGCAAGACTATAAGCCTGTG and ATAATGGGATCTGCAGCGTG to obtain a 252-bp band. All libraries screened were from Life Technologies. For northern blots, single-stranded probes were constructed with the *Not*I/*Bgl*III fragment of the human LTRPC2 sequence as template. Hybridizations were performed using standard methods.

Assays for Nudix activity

Enzyme velocities were quantified by measuring the conversion of a phosphatase-insensitive substrate, ADPR, to the phosphatase-sensitive products, AMP and ribose-5-phosphate. The standard incubation mixture (50 μl) contained 50 mM Tris-Cl buffer (pH 9.0), 16 mM $MgCl_2$, 2 mM ADPR, 0.2–1 milliunits of enzyme and 4 units of alkaline intestinal phosphatase. After 30 min at 37 °C, the reaction was stopped by adding EDTA buffer and inorganic orthophosphate was measured as described[13]. A unit of enzyme hydrolysed 1 μmol of substrate per min under these conditions, and 2 moles of phosphate were liberated per mole of ADPR hydrolysed. The Nudix-type substrates tested included ATP/deoxy-ATP, CTP/deoxy-CTP, GTP/deoxy-GTP, TTP/deoxy-TTP, GDP-mannose, ADP-glucose, UDP-glucose, Ap_nA ($n = 2–6$) (diadenosine polyphosphates, where the number of phosphates are 2–6), NADH, NAD^+, cADPR and ADPR.

The standard assay mixture (without alkaline intestinal phosphatase) was incubated for 30 min at 37 °C and stopped by adding 50 μl of a mixture of four parts of Norit (20% packed volume) and one part of 7% $HClO_4$ to remove adenine-containing nucleotides. After centrifugation, 50 μl was adjusted to an alkaline pH and incubated for an additional 30 min at 37 °C with alkaline intestinal phosphatase to hydrolyse the ribose-5-phosphate formed. The subsequent free phosphate was measured and compared with a control reaction that was not treated with Norit. The stoichiometric relation between the two indicated that the products were AMP and ribose-5-phosphate.

SDS–PAGE and immunoassays

SDS–PAGE, immunoprecipitation and immunoblotting were performed using standard methods or as described in the Figure legends. For immunofluorescence, after 24 h tetracycline induction, HEK-293 cells were fixed (4% paraformaldehyde, 20 min) and permeabilized (0.2% triton X-100, 4 min) before sequential exposure to Hoechst (1 μg ml^{-1}, 2 min) and DioC6 (0.3 μg ml^{-1}, 2 min) (Molecular Probes). For anti-Flag immunofluorescence, cells were blocked and probed with anti-Flag antibody (IBI-Kodak), and then with Alexa 568 goat anti-mouse IgG (Molecular Probes). Mounted samples were imaged using single emission filters (Texas Red, FITC and Hoechst).

Cell culture and electrophysiology

Wild-type and tetracycline-inducible HEK-293 Flag-LTRPC2-expressing cells were cultured at 37 °C with 5% CO_2 in DMEM supplemented with 10% fetal bovine serum and 2 mM glutamine. The medium was supplemented with blasticidin (5 μg ml^{-1}; Invitrogen) and zeocin (0.4 mg ml^{-1}; Invitrogen). Cells were resuspended in medium containing 1 μg ml^{-1} tetracycline (Invitrogen) 24 h before experiments. For patch-clamp experiments, cells were kept in standard Ringer's solution (in mM): 145 NaCl, 2.8 KCl, 1 $CaCl_2$, 2 $MgCl_2$, 10 glucose, 10 HEPES·NaOH (pH 7.2). Standard pipette-filling solutions contained (in mM): 145 Cs-glutamate, 8 NaCl, 1 $MgCl_2$, 10 Cs-BAPTA; 10 HEPES·CsOH (pH 7.2 adjusted with CsOH). In some experiments, $[Ca^{2+}]_i$ was buffered to 100 nM with 10 mM BAPTA and 3.6 mM $CaCl_2$ or left unbuffered. All nucleotides and reagents were purchased from Sigma and dissolved in the standard intracellular solution. Patch-clamp experiments were performed in the whole-cell configuration at 21–25 °C. Data were acquired with 'Pulse' software controlling an EPC-9 amplifier (HEKA). Voltage ramps of 50 ms spanning the voltage range from −100 to +100 mV were delivered from a holding potential of 0 mV at a rate of 0.5 Hz over a period of 200–400 s. When applicable, voltages were corrected for liquid junction potentials. Currents were filtered at 2.9 kHz and digitized at 100 μs intervals. Capacitive currents and series resistance were determined and corrected before each voltage ramp. For analysis, the very first ramps before activating the currents were digitally filtered at 2 kHz, pooled and used for leak-substraction of all subsequent current records. The low-resolution temporal development of currents for a given potential was extracted from the leak-corrected individual ramp current records by measuring the current amplitudes at voltages of −80 mV or +80 mV. Single channels were recorded in the inside-out configuration and currents were filtered and sampled as above. For display purposes, data records were digitally filtered and down-sampled to 100 Hz.

For details of methods used for LTRPC2 and NUDT9 cloning, construction of eukaryotic and prokaryotic expression vector and NUTD9/NUDT9-H purification, see Supplementary Information.

Received 5 December 2000; accepted 16 March 2001.

1. Nagamine, K. *et al.* Molecular cloning of a novel putative Ca^{2+} channel protein (TRPC7) highly expressed in brain. *Genomics* **54,** 124–131 (1998).
2. Harteneck, C., Plant, T. D. & Schultz, G. From worm to man: three subfamilies of TRP channels. *Trends Neurosci.* **23,** 159–166 (2000).
3. Bessman, M. J., Frick, D. N. & O'Handley, S. F. The MuT proteins or 'Nudix' hydrolases, a family of versatile, widely distributed, 'housecleaning' enzymes. *J. Biol. Chem.* **271,** 25059–25062 (1996).
4. Wilding, M., Russo, G. L., Galione, A., Marino, M. & Dale, B. ADP-ribose gates the fertilization channel in ascidian oocytes. *Am. J. Physiol.* **275,** C1277–1283 (1998).
5. Hillyard, D. *et al.* The pyridine nucleotide cycle. Studies in *Escherichia coli* and the human cell line D98/AH2. *J. Biol. Chem.* **256,** 8491–8497 (1981).
6. Dousa, T. P., Chini, E. N. & Beers, K. W. Adenine nucleotide diphosphates: emerging second messengers acting via intracellular Ca^{2+} release. *Am. J. Physiol.* **271,** C1007–1024 (1996).
7. McConkey, D. J. & Orrenius, S. Signal transduction pathways in apoptosis. *Stem Cells* **14,** 619–631 (1996).
8. Koch-Nolte, F. & Haag, F. Mono(ADP-ribosyl)transferases and related enzymes in animal tissues. Emerging gene families. *Adv. Exp. Med. Biol.* **419,** 1–13 (1997).
9. Okazaki, I. J. & Moss, J. Glycosylphosphatidylinositol-anchored and secretory isoforms of mono-ADP-ribosyltransferases. *J. Biol. Chem.* **273,** 23617–23620 (1998).
10. Chakraborti, T., Das, S., Mondal, M., Roychoudhury, S. & Chakraborti, S. Oxidant, mitochondria and calcium: an overview. *Cell. Signal.* **11,** 77–85 (1999).
11. Liang, M., Chini, E. N., Cheng, J. & Dousa, T. P. Synthesis of NAADP and cADPR in mitochondria. *Arch. Biochem. Biophys.* **371,** 317–325 (1999).
12. Guse, A. H. Cyclic ADP-ribose. *J. Mol. Med.* **78,** 26–35 (2000).
13. Ames, B. N. & Dubin, D. T. The role of polyamines in the neutralization of bacteriophage deoxyribonucleic acid. *J. Biol. Chem.* 769–775 (1960).

Supplementary information is available on *Nature*'s World-Wide Web site (http://www.nature.com) or as paper copy from the London editorial office of *Nature*.

Acknowledgements

We thank D. Tani and M. Monteilh-Zoller for technical assistance. This work was funded in part by a Beth Israel Pathology Foundation grant, a BIDMC Fireman Fellowship award to A.M.S. and NIH grants to A.M.S. and M.J.B. A.L.P. is supported by the German Academic Exchange Service (DAAD). In memory of Q. Zhu.

Correspondence and requests for materials should be addressed to A.M.S. (e-mail: andrewms@u.washington.edu). The GenBank accession number for NUDT9 cDNA and protein sequences is AY026252.

Association of NOD2 leucine-rich repeat variants with susceptibility to Crohn's disease

Jean-Pierre Hugot*†‡, Mathias Chamaillard*†, Habib Zouali*, Suzanne Lesage*, Jean-Pierre Cézard‡, Jacques Belaiche§, Sven Almer‖, Curt Tysk¶, Colm A. O'Morain#, Miquel Gassull☆, Vibeke Binder, Yigael Finkel††, Antoine Cortot‡‡, Robert Modigliani§§, Pierre Laurent-Puig†, Corine Gower-Rousseau‡‡, Jeanne Macry‖‖, Jean-Frédéric Colombel‡‡, Mourad Sahbatou* & Gilles Thomas*†¶¶**

** Fondation Jean Dausset CEPH, 27 rue J. Dodu 75010 Paris, France*
† INSERM U434, 27 rue J. Dodu 75010 Paris, France
‡ PEWG-IBD, Department of Paediatric Gastroenterology, Hôpital Robert Debré, 75019 Paris, France
§ GETAID and Department of Gastroenterology, CHU de Liège, 4000 Belgium
‖ Division of Gastroenterology and Hepatology, IHM, Linköpings Universitet, SE-581 85 Linköping, Sweden
¶ Department of Gastroenterology, Örebro Medical Center Hospital, SE-701 85 Örebro, Sweden
 # Department of Gastroenterology, Adelaide & Meath Hospital, Dublin 24, Ireland
☆ Department of Gastroenterology, Hospital Universitari Germans Trias i Pujol, Badalona, 08916 Spain
*** Department of Gastroenterology Herlev Hospital, 2730 Herlev, Denmark*
†† Astrid Lindgren Children's Hospital, SE-161 76 Stockholm, Sweden
‡‡ Registre EPIMAD, Hôpital Calmette, 59037 Lille, France
§§ Department of Gastroenterology, Hopital Saint Louis, 75475 Paris, France
‖‖ INSERM U458, Hôpital Robert Debré, 75019 Paris, France
¶¶ Department of Surgery, Hôpital Saint Antoine, 75012 Paris, France

Crohn's disease[1,2] and ulcerative colitis, the two main types of chronic inflammatory bowel disease, are multifactorial conditions of unknown aetiology. A susceptibility locus for Crohn's disease has been mapped[3] to chromosome 16. Here we have used a positional-cloning strategy, based on linkage analysis followed by linkage disequilibrium mapping, to identify three independent associations for Crohn's disease: a frameshift variant and two missense variants of *NOD2*, encoding a member of the Apaf-1/Ced-4 superfamily of apoptosis regulators that is expressed in monocytes. These *NOD2* variants alter the structure of either the leucine-rich repeat domain of the protein or the adjacent region. NOD2 activates nuclear factor NF-kB; this activating function is regulated by the carboxy-terminal leucine-rich repeat domain, which has an inhibitory role and also acts as an intracellular receptor for components of microbial pathogens. These observations suggest that the *NOD2* gene product confers susceptibility to Crohn's disease by altering the recognition of these components and/or by over-activating NF-kB in monocytes, thus documenting a molecular model for the pathogenic mechanism of Crohn's disease that can now be further investigated.

Crohn's disease (CD; MIM 266600) occurs primarily in young adults, with an estimated prevalence of 1 in 1,000 in western countries[1]. Its incidence has increased markedly over the past half century, arguing for the involvement of recent, unidentified, environmental factors[2]. Familial aggregation of the disease suggests that genetic factors may also be involved—an hypothesis that was substantiated in 1996 by the discovery of a susceptibility locus for CD, *IBD1*, on chromosome 16 (ref. 3). Identification of the exact nature of the genetic changes that are implicated in CD susceptibility would provide a specific approach to understanding this common disorder.

Because candidate genes previously localized on chromosome 16 failed to show an association with CD[4,5], we refined the localization of the *IBD1* susceptibility locus by typing 26 microsatellite markers spaced at an average distance of 1 cM in the pericentromeric region

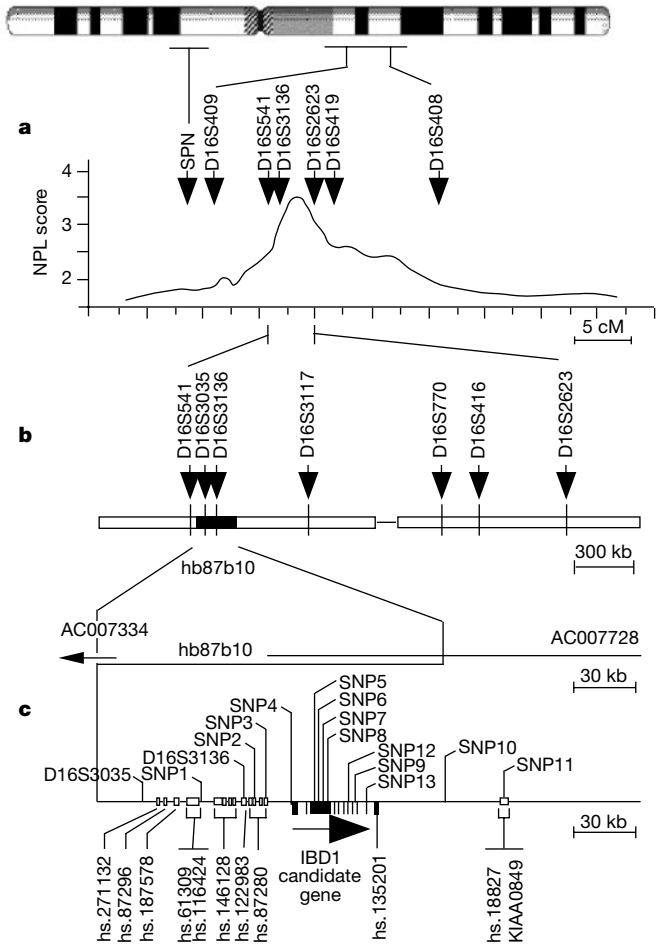

Figure 1 Strategy used to identify the *IBD1* locus. **a**, Profile for the multipoint non-parametric linkage (NPL) scores. Approximate cytogenetic localizations are shown for selected microsatellite markers used in the study[3] that localized *IBD1* to the pericentromeric region of chromosome 16. Subsequent linkage analyses were focused on the region between SPN and D16S408. The highest NPL score (maximum NPL score, 3.49; $P = 2.37 \times 10^{-4}$) was in the region between markers D16S541 and D16S2623 (ref. 6). **b**, Physical map of the *IBD1* region[6]. White and black boxes correspond to the two BAC contigs and BAC clone hb87b10, respectively. Five yeast artificial chromosomes (YACs) bridge a gap of ~100 kb between these two contigs. The position on the physical map of the microsatellite markers used in the linkage analysis is indicated. Distance between D16S541 and D16S2623 is ~2 Mb. **c**, Representation of the sequenced region containing the *IBD1* candidate gene. Unigene clusters and 11 exons of the *IBD1* candidate gene are indicated by white and black boxes, respectively. Bold horizontal arrow indicates direction of transcription. Positions of SNP 1–13, D16S3035 and D16S3136, which were typed in 235 CD families for linkage disequilibrium studies, are shown.